

NeuralCRNs: A Natural Implementation of Learning in Chemical Reaction Networks

Rajiv Teja Nagipogu^{1*}, John H. Reif¹,

¹ Department of Computer Science, Duke University, Durham, NC 27708, United States

* Corresponding author

E-mail: rajivteja.nagipogu@duke.edu

Author contributions

Rajiv Teja Nagipogu (RN) and John H. Reif (JR) jointly conceived the idea for the problem statement on obtaining more chemically natural learning implementations. RN conceived the solution, performed the simulations, and wrote the manuscript. John supervised the work and also edited the manuscript.

Abstract

The remarkable ability of single-celled organisms to sense and react to the dynamic changes in their environment is a testament to the adaptive capabilities of their internal biochemical circuitry. One of the goals of synthetic biology is to develop biochemical analogues of such systems to autonomously monitor and control biochemical processes. Such systems may have impactful applications in fields such as molecular diagnostics, smart therapeutics, and *in vivo* nanomedicine. So far, the attempts to create such systems have been focused on functionally replicating the behavior of traditional feedforward networks in abstract and DNA-based synthetic chemistries. However, the inherent incompatibility between digital and chemical modes of computation introduces several nonidealities into these implementations, making it challenging to realize them in practice. In this work, we present NeuralCRNs, a novel supervised learning framework constructed as a collection of deterministic chemical reaction networks (CRNs). Unlike prior works, the NeuralCRNs framework is founded on dynamical system-based learning implementations and, thus, results in chemically compatible computations. First, we show the construction and training of a supervised learning classifier for linear classification. We then extend this framework to support nonlinear classification. We then demonstrate the validity of our constructions by training and evaluating them first on several binary and multi-class classification datasets with complex class separation boundaries. Finally, we detail several considerations regarding the NeuralCRNs framework and elaborate on the pros and cons of our methodology compared to the existing works.

1 Introduction

Learning and adaptation are fundamental features of living organisms and allow them to sense, respond to, and adapt in continuously changing environments [1]. In broad terms, we define *learning* as the process through which an organism acquires knowledge of its surroundings through experience and feedback. The organism then utilizes this knowledge to make decisions under uncertainty. Higher vertebrates evolved specialized structures (e.g., neuronal brains) for this purpose owing to the complexity of their tasks. In contrast, despite the lack of such sophisticated organs, single-celled organisms exhibit rudimentary forms of learning. Examples include classical conditioning in *Paramecium* [2] and bacterial chemotaxis [3]. In addition, the demonstration of associative learning through a gene regulatory network embedded within *Escherichia coli* [4] and the implementation of associative memories through an *in vitro* transcriptional circuit [5], among others, show that simple biochemical circuits are capable of intelligent behavior [6].

In this work, we tackle the problem of *chemical learning*—the prospect of constructing chemical reaction systems capable of autonomous neural network-like learning and inference. Much like how neural networks could be trained to associate input data patterns with their class labels, chemical learning systems can self-adjust their internal state through environmental feedback to associate chemical signal patterns with the environment’s state. We are motivated by the ongoing progress in the field of biomolecular computing in constructing increasingly complex computational circuits using DNA-based synthetic chemistries [7–18]. Although our constructions primarily use abstract reaction systems, we keep in mind the current capabilities and physical limitations of DNA nanotechnology [13, 19] while designing the circuits, setting the groundwork for a future DNA implementation.

Many chemical pattern classification tasks could be accomplished by simply imitating (chemically) a neural network trained *in silico* [14, 16, 20]. What, then, is the need for learning in the chemical medium? The answer to this question is multifaceted. First, biological information processing tasks, including learning and a host of other processes that make life possible, occur through chemical means. Understanding chemical learning could provide a window into the sophistication of biochemical learning. Second, a learnable system is reprogrammable, i.e., it could be retrained and repurposed for different tasks *in situ*, voiding the need to design an entirely new system for each new task [21]. Finally, a learnable system can function in noisy chemical environments, quickly adapting to the fluctuations in the chemical signal patterns, thus eliminating the need for external intervention (e.g., as a decision-making circuit in future artificial life systems [22]). We believe that the effect of chemical learning on chemical computing would be qualitatively comparable to the advancements enabled by neural networks in digital computing [23–25].

In fact, existing attempts at building adaptive molecular systems have largely resorted to reproducing the functionality of classical neural networks [26], such as perceptrons [15, 21, 27, 28] and multi-layer feedforward networks [29–31]. Banda *et al.* [27, 28] presented several trainable “chemical” perceptron systems using enzyme-based artificial chemistries. Lakin *et al.* [15, 21] presented two physical realizations of the perceptron learning algorithm first through a DNAzyme-based implementation [32] and later through the “buffered” strand displacement gate motif. Blount *et al.* [29] designed a multi-layer feedforward network by improving upon the perceptron designs from [27, 28]. Arredondo *et al.* [30] simulated a similar network but serialized its operations using a molecular clock circuit to minimize the implementation complexity. They further presented the chemical implementation of the so-called weight perturbation algorithm to train their network. Several other neural network constructions were also realized in the chemical medium involving presupposed weights or weights trained *in silico*. These include the chemical implementation of a McCulloch-Pitts neuron [33] for computing boolean functions [34], a “winner-take-all” circuit [16] for pattern recognition, and a *ReLU*-activated feedforward neural network implemented using non-competitive CRNs [20].

However, the inherent incompatibility between the digital and chemical modes of computation introduces several nonidealities in these chemical implementations. For example, consider how the multiplication is implemented in each of these networks. The multiplication CRN is an equilibrium system that is only accurate once the system reaches a steady state. Since input-weight multiplication is the major operation in neural networks, their chemical implementations would require a host of bookkeeping modules to monitor the reaching of the steady state and synchronization modules to coordinate among the multiplication CRNs at different network nodes. These additions significantly raise the circuit complexity, making the physical realizations of these systems hard. Further, these implementations require stricter control over the rate constants in the underlying rate constant [27, 28], which also imparts a significant design overhead.

Tackling these issues, we present NeuralCRNs, an alternative approach to implementing chemical learning using continuous-time analog computations. The NeuralCRNs framework is founded upon a special class of dynamical system-based neural systems known as Neural ordinary differential equations (NeuralODEs for short) [35]. NeuralODEs model neural computations as solutions to the initial value problems (IVPs) of a set of ordinary differential equations (ODEs). In this sense, the NeuralCRNs represent a subclass of NeuralODEs in which the ODEs correspond to the mass action kinetics of a CRN system. The NeuralCRNs can then be constructed by converting these ODEs into CRNs. Since solving the IVP of an ODE is equivalent to running the corresponding CRN in a given time frame, the computations in our framework are chemically compatible and are thus expected to result in succinct and simpler reaction networks. The main contributions of this work are as follows:

- We show the construction of supervised learning classifiers using the NeuralCRNs framework for both linear and nonlinear classification (§3.1 and §3.3).
- We describe the different steps in training the NeuralCRN classifiers and suggest ways to optimize the training procedure using a minimum number of sequential steps (§3.2).
- We then simulate the training and evaluation process on various classification tasks to demonstrate the validity of our constructions and the training process (§4).
- We conclude by elaborating on various design decisions. Here, we also compare and contrast the NeuralCRNs framework with that of the earlier works (§5).

2 Background

2.1 Supervised learning in Artificial Neural Networks

Artificial neural networks (ANNs) are layered graph structures with weighted bipartite connections between the nodes of successive layers. The input-to-output computation in these networks flows in a single direction from the initial layer to the final layer. For this reason, they are sometimes also referred to as *feedforward* neural networks (FFNNs). Typically, ANNs learn through a method known as *gradient descent* [25], where the weighted connections are adjusted iteratively, informed by the gradients of their prediction error.

In this work, we utilize the *supervised learning* variant [24] for training our models. The defining characteristic of this variant is the presence of a labeled dataset—tuples containing a data point and a class label—where the class label speaks to the nature of the data point. Let $\mathcal{D} = \{(\mathbf{x}_1, y_1), (\mathbf{x}_2, y_2), \dots, (\mathbf{x}_N, y_N)\}$ be the dataset on which the ANN is being trained with x_i as the data points and y_i as the class labels. Further, let $\hat{\theta}$ be the current parameter set of the network and $f_{\hat{\theta}}$ be the current parameterized transformation function.

Each training iteration in gradient descent consists of two main phases: (i) the forward phase and (ii) the backpropagation phase. In the *forward* phase, the network computes the output \hat{y}_i for the given input x_i by applying its transformation function $f_{\hat{\theta}}$

$$\hat{y} = f_{\hat{\theta}}(x_i).$$

In the *backpropagation* phase, the loss \mathcal{L} of the current prediction \hat{y}_i with respect to the expected value y_i is estimated. Then, the loss gradients $g_{\hat{\theta}_i}$ are computed as the partial differential of \mathcal{L} with respect to each parameter $\hat{\theta}_i$ through a recursive technique known as automatic differentiation [36]. These loss gradients are then utilized to update the parameter values.

$$\begin{aligned} \mathcal{L} &= \frac{1}{2}(\hat{y}_i - y)^2 \\ g_{\hat{\theta}_i} &= \frac{\partial \mathcal{L}}{\partial \hat{\theta}_i} \\ \hat{\theta}_i^{new} &= \hat{\theta}_i^{old} - \eta g_{\hat{\theta}_i} \end{aligned} \tag{1}$$

where η represents the learning rate hyperparameter that specifies the speed at which the network learns.

Multiple such training iterations are performed over the entire dataset, ensuring that the loss decreases steadily until it finally converges. The network is then declared to be “trained”, after which it is employed to classify previously unclassified inputs. Through this process, the network encodes implicit patterns within its training data distribution into its parameters and uses the gained knowledge to accurately classify previously unseen examples.

2.2 Chemical Reaction Networks

A *chemical reaction network* (CRN) is an abstract mathematical formalism used to model the dynamics of a set of coupled chemical reactions. It is formally represented as a tuple $(\mathcal{S}, \mathcal{R})$, where \mathcal{S} represents the abstract chemical species, \mathcal{R} represents the set of reactions involving the species in \mathcal{S} . Each element $r(\alpha, \beta, k) \in \mathcal{R}$ represent the chemical reaction



where $\alpha \in \mathcal{S}$ and $\beta \in \mathcal{S}$ are multisets representing the reactants and products of r , respectively, and k represents its rate constant.

In this work, we work exclusively with deterministic CRNs, whose dynamics could be described by the laws of mass action kinetics—the reactions occur in a well-mixed solution, and all the species are present at high enough concentrations. The rate equations for the individual species involved in the reaction are represented using the following set of differential equations [37].

$$\frac{d\beta_j}{dt} = k \prod_s \alpha_s \tag{2}$$

$$\frac{d\alpha_i}{dt} = -k \prod_s \alpha_s \tag{3}$$

Note that, in this formulation of the rate law, there can be duplicates among α_i ’s and β_j ’s, and the effective dynamics of a specific species should be derived by combining all its equations in the enumerated set.

2.3 An overview of NeuralODEs

As discussed before, NeuralODEs [35] are continuous-time neural networks that model neural computations—calculations of the hidden state and the gradients—as solutions to the IVPs of a set of ODE systems. Here, we briefly outline the different ODE systems involved in the NeuralODEs framework.

The *forward* phase in NeuralODEs models the evolution of the hidden state \mathbf{z} starting from input \mathbf{x} at time $t = 0$ to its final state at $t = T$. Eq. (4) shows the temporal dynamics of \mathbf{z} defined by the hidden state dynamics function f_θ parameterized by θ representing the NeuralODE parameters. Eq. (5) represents the corresponding IVP, usually solved using a blackbox ODE solver [38–40].

$$\frac{d\mathbf{z}(t)}{dt} = f_\theta(\mathbf{x}, \mathbf{z}) \quad \mathbf{x} = \mathbf{z}(0) \tag{4}$$

$$\mathbf{z}(T) = \mathbf{z}(0) + \int_0^T f_\theta(\mathbf{x}, \mathbf{z}) dt. \tag{5}$$

The *backpropagation* phase in NeuralODEs utilizes a technique known as the *adjoint sensitivity* method [41] to calculate the parameter gradients $\frac{\partial \mathcal{L}}{\partial \theta}$, where \mathcal{L} represents the loss. First, the method introduces a variable known as the *adjoint* defined as the partial differential of \mathcal{L} with respect to \mathbf{z} : $\mathbf{a}(t) = \frac{\partial \mathcal{L}}{\partial \mathbf{z}}(t)$. Then, the gradients are estimated by simultaneously solving three backpropagation ODEs in the reverse time, i.e., from $t = T$ to $t = 0$: (i) hidden state backpropagation (6), (ii) adjoint state backpropagation (7), and (iii) gradient backpropagation (8).

$$\frac{dz}{dt} = -f_{\theta}(z) \quad (6)$$

$$\frac{d\mathbf{a}(t)}{dt} = -\mathbf{a}(t)^T \frac{\partial f_{\theta}}{\partial \mathbf{z}} \quad (7)$$

$$\frac{d}{dt} \frac{\partial \mathcal{L}}{\partial \theta} = -\mathbf{a}(t)^T \frac{\partial f_{\theta}}{\partial \theta} \quad (8)$$

Briefly put, the gradients start from zero at $t = T$ and evolve into their final state at $t = 0$. The three backpropagation ODE systems represent the evolution of the gradients along with their dependent variables, viz. \mathbf{z} and \mathbf{a} . In the backpropagation of \mathbf{z} , the vector \mathbf{z} flows from its final state to its initial state, retracing its flow in the forward phase. In the backpropagation of \mathbf{a} , the vector \mathbf{a} flows from its initial state ($\mathbf{a}_{init} = \frac{\partial \mathcal{L}}{\partial \mathbf{z}}(T)$) to its final state according to (7). The final gradient values are then used to update the parameters θ according to (1).

2.4 From ODEs to CRNs

Recall that we derive the NeuralCRNs framework by converting the ODEs from the NeuralODEs framework into their equivalent CRNs guided by mass action kinetics. In this work, we utilize the *Hungarian lemma* [37] to perform this conversion. This lemma specifies the procedure to convert a special subclass of polynomial ODEs known as Hungarian ODEs into CRNs. A *Hungarian ODE* system is characterized by (a) non-negative variables and (b) the presence of the differential variable of the ODE in all the negative monomials on the right-hand side [42]. We also employ the *dual-rail* encoding to recast the non-Hungarian ODE systems that would appear during the translation into a Hungarian system, as suggested by [42, 43]. Each monomial in the Hungarian ODE is then converted into a single chemical reaction as follows: (a) the factor variables in the monomial become the reactants, (b) the differential variable becomes a product, and (c) the reaction is designed to be catalytic in its reactants.

The dual-rail encoding represents each variable as the difference between two complementary variables corresponding to the positive and negative parities. Each dual-rail variable is assigned a single chemical species whose concentration represents the variable’s value. Below, we show the translations of three different ODE systems named Type-I-ODE, Type-II-ODE, and Type-III-ODE, which will later be the building blocks for constructing our NeuralCRNs. In what follows, we use the lowercase alphabet to denote algebraic variables and their uppercase counterparts to designate the corresponding chemical species. The $+/-$ in the superscript represents the positive and negative parities of the dual-rail notation.

Type-I-ODE. $\frac{dz}{dt} = xy$, where $x, y, z \in \mathbb{R}_{>0}$, represents a Hungarian ODE with a single monomial. The translation of the monomial into its corresponding reaction is shown in Table 1.

Table 1. ODE to CRN translation of Type-I-ODE.

ODE	CRN
$\frac{dz}{dt} = xy, \quad x, y, z \geq 0$	$X + Y \rightarrow Z + X + Y$

Type-II-ODE. $\frac{dz}{dt} = xy$, where $x, y, z \in \mathbb{R}$, represents a non-Hungarian ODE system. Therefore it is first

converted into a Hungarian system by rewriting it in the dual-rail format and then translated into a CRN.

$$\frac{dz}{dt} = xy \tag{9}$$

$$\frac{d(z^+ - z^-)}{dt} = (x^+ - x^-)(y^+ - y^-) \tag{10}$$

$$\frac{dz^+}{dt} = x^+y^+ + x^-y^- \tag{11}$$

$$\frac{dz^-}{dt} = x^+y^- + x^-y^+ \tag{12}$$

where $x^+, x^-, y^+, y^-, z^+, z^- > 0$. Observe that the dual-rail encoding results in four Type-I-ODEs, resulting in four chemical reactions.

Type-III-ODE. $\frac{dz}{dt} = -xy$, where $x, y, z \in \mathbb{R}$ follows a similar translation process as the Type-II-ODE as shown below:

$$\frac{d(z^+ - z^-)}{dt} = -(x^+ - x^-)(y^+ - y^-) \tag{13}$$

$$\frac{dz^+}{dt} = x^+y^- + x^-y^+ \tag{14}$$

$$\frac{dz^-}{dt} = x^+y^+ + x^-y^- \tag{15}$$

where $x^+, x^-, y^+, y^-, z^+, z^- > 0$ results in four Type-I-ODEs and, by extension, four reactions, one for each monomial.

CRNs for Arithmetic Operators

In addition to the above translations, we also utilize the CRNs for the arithmetic operators of addition (`crn_add`), subtraction (`crn_subtract`), and multiplication (`crn_multiply`), as shown in Table 2. These CRNs each simulate the arithmetic operations $y = a + b$, $y = a - b$, and $y = a * b$, respectively, with $a, b, y \in \mathbb{R}$.

Table 2. CRNs for arithmetic operations.

Addition (<code>crn_add</code>)	Subtraction (<code>crn_subtract</code>)	Multiplication (<code>crn_multiply</code>)
$A^+ \rightarrow Y^+$	$A^+ \rightarrow Y^+$	$A^+ + B^+ \rightarrow Y^+ + A^+ + B^+$
$B^+ \rightarrow Y^+$	$A^- \rightarrow Y^-$	$A^- + B^- \rightarrow Y^- + A^- + B^-$
$A^- \rightarrow Y^-$	$B^+ \rightarrow Y^-$	$A^+ + B^- \rightarrow Y^- + A^+ + B^-$
$B^- \rightarrow Y^-$	$B^- \rightarrow Y^+$	$A^- + B^+ \rightarrow Y^+ + A^- + B^+$
		$Y^+ \rightarrow 0$
		$Y^- \rightarrow 0$

CRNs for addition, subtraction, and multiplication in the dual-rail format adapted from [44, 45]. They calculate $y = a + b$, $y = a - b$, and $y = a * b$, respectively. The output could be read out from the concentrations of Y^+ and Y^- at the steady state (*ss*): $y = [Y^+]_{ss} - [Y^-]_{ss}$.

3 NeuralCRNs for supervised learning

In this section, we describe the construction and training of supervised learning classifiers in the NeuralCRNs framework. First, we instantiate the NeuralODEs framework with an appropriate choice of dynamics function f_θ and enumerate the resulting ODEs. Then, we use the ODE to CRN translation templates presented in §2.4 to convert these ODEs into CRNs. Finally, we repurpose this framework into a supervised learning classifier and describe its training procedure. Note that the choice of f_θ is critical in determining the approximation abilities of the constructed classifier. In this work, we construct two classifiers corresponding to two different choices of f_θ : (i) Linear-NeuralCRN and (ii) Nonlinear-NeuralCRN. Briefly, the *Linear-NeuralCRN* can

approximate linear separation boundaries between classes, while the Nonlinear-NeuralCRN can approximate nonlinear separation boundaries. Before delving into the construction, we make a few assumptions regarding the classifiers and the NeuralCRNs framework to simplify the discussions; we describe briefly how they could be relaxed whenever necessary.

1. We work with a two-dimensional (2D) NeuralCRNs framework in the initial constructions. Later, we will show how this system can be extended into a higher dimensional system.
2. We consider binary classification tasks (*positive* class: 1 and *negative* class: 0) during the construction and extend it to multi-class classification in the later sections. Further, we use the logistic regression [46] formulation of binary classification: the output \hat{y} is a scalar variable, and the class label is determined by comparing \hat{y} with a predefined threshold Th as shown below

$$label = \begin{cases} 1 & \hat{y} > Th \\ 0 & \text{otherwise.} \end{cases}$$

Note that the values ‘1’ and ‘0’ for the positive and negative classes are arbitrary and could change depending on the task.

3. Symbols in lowercase represent algebraic variables, whereas their uppercase counterparts represent the chemical species corresponding to the variable.
4. All the CRNs and the algebraic variables are specified in the dual-rail encoding. The + or – in the variable’s superscript denotes its positive or negative parity. However, in the interest of clarity and conciseness, we sometimes use a short-hand notation, for example, “the Z species” or “the hidden state species Z ” to collectively reference a set of states.
5. The concentrations of the dual-rail chemical species are initialized as follows. If X is the chemical species corresponding to the variable x , then

$$\begin{aligned} [X^+]_{t=0} &= \max(0, x) \\ [X^-]_{t=0} &= \max(0, -x). \end{aligned}$$

In some places, we also use the short-hand form $X \leftarrow x$ to represent this initialization.

6. The forward phase is assumed to run from time $t = 0$ to $t = T$. In NeuralODEs, the backpropagation phase runs in reverse time, i.e., from $t = T$ to $t = 0$. However, since CRNs cannot run in reverse time, the parities of the ODEs in the backpropagation stage are inverted before being inducted into the NeuralCRNs framework.
7. Our constructions assume the presence of a chemical oscillator circuit that functions as a sequencer (or a clock) that switches the control from the current step to the next when the oscillator cycle changes [45].
8. Our classifier architecture comprises a NeuralCRN layer and a final classification layer. Here, we assume that the NeuralCRNs framework can model the required I/O transformation function. Therefore, we *freeze* the weights in the final layer, i.e., keep them constant throughout the training process.
9. We use the terms *linear classifier* and *nonlinear classifier* to mean classifiers that can discriminate data points between classes with linear and nonlinear separation boundaries, respectively.
10. We assume that creating copies of species is fast. We represent the species assumed to be copied using an asterisk (*) in their superscripts.

3.1 Linear NeuralCRN

We use $f_{\theta}^{linear}(\mathbf{z}) = \theta\mathbf{z}, \theta \in \mathbb{R}^{2 \times 2}, \mathbf{z} \in \mathbb{R}^2$ as the hidden state dynamics function for constructing the Linear-NeuralCRN. While this is not the most optimal choice of dynamics function for a linear classifier, we opted for it because it generates simpler notation to outline the general ideas. We provide a much simpler implementation of the Linear-NeuralCRN in SI text S2. The computations in NeuralODEs (and therefore in NeuralCRNs) are homeomorphisms that preserve the dimension throughout their operation. Since we assume the logistic regression formulation of binary classification, the final output should be a single scalar variable. To achieve this, we stack the NeuralCRN layer with a perceptron-like *classification layer* (alternately referred to as the final layer or final classification layer), which computes the weighted sum of the final hidden state components of the NeuralCRN layer. As mentioned before, the weights of this final layer are frozen. Fig 1 compares our Linear-NeuralCRN framework (left) with a qualitatively equivalent feedforward neural network (right).

Now we will enumerate different steps involved in constructing the Linear-NeuralCRN and specify their CRNs. We designate each step using the short-hand notation CRN_f^i and CRN_b^i , denoting the i^{th} step in the forward (denoted by f in the subscript) and backpropagation (denoted by b in the subscript) phases. Later, we will show how some of these CRNs could be merged to reduce the number of sequential steps in a training iteration.

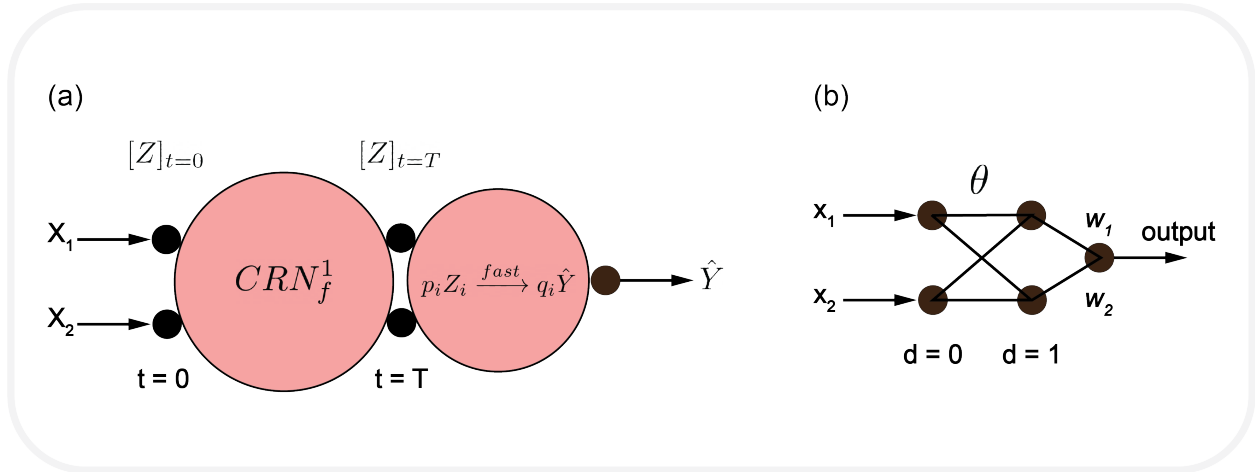


Fig 1. A comparison of the Linear-NeuralCRN architecture with a qualitatively similar feedforward neural network architecture.

(a) Architecture of the Linear-NeuralCRN. The first layer (circle) is the NeuralCRN layer that models the hidden state evolution from $t = 0$ to $t = T$. The second layer (circle) is the final layer that converts the hidden state species Z into the output species \hat{Y} . (b) A feedforward neural network analogous to the Linear-NeuralCRN. The NeuralCRN layer in the Linear-NeuralCRN could theoretically approximate the calculations performed by the first layer in the network [17].

Evolution of the hidden state species (CRN_f^1). This CRN models the evolution of the hidden state species Z starting from a concentration given by the network input at $t = 0$ to its final state at $t = T$. Eq. (16) shows the expanded ODE system obtained by substituting f_{θ}^{linear} as the dynamics function in (4).

$$\begin{aligned} \frac{d\mathbf{z}(t)}{dt} &= f_{\theta}^{linear}(\mathbf{z}) = \theta\mathbf{z} \\ \begin{bmatrix} \frac{dz_1}{dt} \\ \frac{dz_2}{dt} \end{bmatrix} &= \begin{bmatrix} \theta_{11} & \theta_{12} \\ \theta_{21} & \theta_{22} \end{bmatrix} \begin{bmatrix} z_1 \\ z_2 \end{bmatrix} = \begin{bmatrix} \theta_{11}z_1 + \theta_{12}z_2 \\ \theta_{21}z_1 + \theta_{22}z_2 \end{bmatrix} \end{aligned} \quad (16)$$

Since we assume that $\mathbf{z} \in \mathbb{R}^2$ and $\theta \in \mathbb{R}^{2 \times 2}$, each monomial in (16) is a Type-II-ODE which translates to four dual-rail reactions as shown in Table 3. The first two columns show the ODE and its CRN translation, and the third column shows how the species are initialized according to Assumption 5.

Table 3. Forward phase CRN of the NeuralCRNs framework.

ODE	CRN	Initialization ($t = 0$)
$\frac{dz_i}{dt} = \theta_{ij} z_j$	$P_{ij}^+ + Z_j^+ \rightarrow Z_i^+ + P_{ij}^+ + Z_j^+$	$P_{ij} \leftarrow \theta_{ij}$
	$P_{ij}^- + Z_j^- \rightarrow Z_i^- + P_{ij}^- + Z_j^-$	
	$P_{ij}^+ + Z_j^- \rightarrow Z_i^- + P_{ij}^+ + Z_j^-$	$Z_i \leftarrow x_i$
	$P_{ij}^- + Z_j^+ \rightarrow Z_i^+ + P_{ij}^- + Z_j^+$	

ODE to CRN translation for the hidden state evolution showing the ODE monomial in the first column, the expanded CRN in the second column, and the corresponding species initialization in the third column.

Creation of the output species (CRN_f²). This CRN transforms the hidden state species Z at the end of the previous step into the output species \hat{Y} . Recall that the final output \hat{y} is calculated as the weighted sum of hidden state components (17). Without loss of generality, we assume that the final layer weights are rational, i.e., $w_i = \frac{p_i}{q_i}$. Then, we utilize the rational multiplication CRN from [20] to generate the output species as shown in (18).

$$\hat{y} = \sum_i w_i z_i \quad i = \{1, 2\} \quad (17)$$

$$q_i Z_i \rightarrow p_i \hat{Y} \quad w_i = \frac{p_i}{q_i} \quad (18)$$

Creation of the error species (CRN_b¹). This CRN creates the error species E corresponding to the *deviation error* e —the difference between the predicted output \hat{y} and the target output y (19). They are created as output species of the `crn_subtract` CRN between the predicted output species \hat{Y} and the target output species Y (20). The E species are used to generate the adjoint species in the next step.

$$e = \hat{y} - y \quad (19)$$

$$E \leftarrow \text{crn_subtract}(\hat{Y}, Y). \quad (20)$$

Creation of the adjoint species (CRN_b²). This CRN facilitates the creation (or initialization) of the adjoint species A , necessary for modeling the evolution of the gradient species in the next step. Using the *squared loss* (21) as our loss function, the adjoint species are initialized as the product of e and the final layer weights w_i . In CRN terms, this once again translates into a rational multiplication CRN [20] between the W (corresponding to w_i) and E species, creating the A species as products (23).

$$\mathcal{L} = \frac{1}{2}(\hat{y} - y)^2 \quad (21)$$

$$\mathbf{a}(T) = \frac{\partial \mathcal{L}}{\partial \mathbf{z}} = (\hat{y} - y) \frac{\partial \hat{y}}{\partial \mathbf{z}}$$

$$a_i(T) = e w_i \quad \frac{\partial \hat{y}}{\partial z_i} = w_i \text{ from (17)} \quad (22)$$

$$q_i E^* \rightarrow p_i A_i \quad w_i = \frac{p_i}{q_i}, i = 1, 2. \quad (23)$$

Here, E^* represents that the E species have been duplicated for the creation of different A_i species.

Evolution of the gradient species (CRN_b³). This CRN models the evolution of the gradient species G by simultaneously running three backpropagation CRNs: (a) hidden state backpropagation, (b) adjoint state backpropagation, and (c) gradient backpropagation (see (6)-(8)). Table 4 shows the construction of each of these CRNs. The first row shows the reverse-time ODEs from the NeuralODE framework. Their parities are inverted in the second row to make them run in forward time to be converted into CRNs. In the second row, the parities of these ODEs are inverted to make them run in forward time so that they can be converted into CRNs. The third row shows the enumerated forms of each ODE from the second row. The fourth row specifies the initial concentrations of the involved species: (a) Z_{init} for the hidden state

species is set to the concentrations of the hidden state species Z at $t = T$; (b) A_{init} for the adjoint species is assigned as shown in (22); and (c) G_{init} for the gradient species is set to zero. The fifth row specifies the ODE-to-CRN translation template to use for converting the enumerating ODEs in the third row into CRNs.

Table 4. Backpropagation CRNs of the NeuralCRNs framework.

S. No	Remark	Hidden state	Adjoint	Gradient
1	$T \rightarrow 0$	$\frac{dz}{dt} = \theta z$	$\frac{da}{dt} = -a^T \frac{\partial f_\theta}{\partial z}$	$\frac{d}{dt} \frac{\partial \mathcal{L}}{\partial \theta} = -a^T \frac{\partial f_\theta}{\partial \theta}$
2	$0 \rightarrow T$	$\frac{dz}{dt} = -\theta z$	$\frac{da}{dt} = a^T \theta$	$\frac{d}{dt} \frac{\partial \mathcal{L}}{\partial \theta} = a^T \frac{\partial f_\theta}{\partial \theta}$
3	RHS Expansion	$-\begin{bmatrix} \theta_{11} & \theta_{12} \\ \theta_{21} & \theta_{22} \end{bmatrix} \begin{bmatrix} z_1 \\ z_2 \end{bmatrix}$	$[a_1 \ a_2] \begin{bmatrix} \theta_{11} & \theta_{12} \\ \theta_{21} & \theta_{22} \end{bmatrix}$	$[a_1 \ a_2] \begin{bmatrix} z_1 & z_2 & 0 & 0 \\ 0 & 0 & z_1 & z_2 \end{bmatrix}$
4	Initial concentration	$Z_{init} \leftarrow z(T)$	$A_{init} \leftarrow ew_i$	$G_{init} \leftarrow 0$
5	Translation	Type-III-ODE	Type-II-ODE	Type-II-ODE

The three backpropagation CRNs that should be run simultaneously to calculate the gradients. They correspond to the time evolution of the gradients and their dependent variables. (Row 1) Reverse-time ODE systems in the NeuralODEs framework. (Row 2) ODE systems from the previous row but with parities inverted, thus running in forward time. (Row 3) Enumerated ODEs of ODE systems in the previous row. (Row 4) Initial concentration assignment of the differential variables in each ODE system. (Row 5) Template to use for translating the ODE into CRN.

Update of the parameter species (CRN⁴_b). This CRN models the update of the parameter species P via the gradient species G through the gradient descent update rule: $\theta_{new} = \theta_{old} - \eta g_\theta$, where θ^{old} and θ^{new} represent the parameter values before and after the update, η represents the learning rate, and g_θ represents the corresponding gradient value. The gradient rule involves two operations: (i) rational multiplication of η and g_θ , and (ii) reduction in the concentration of the parameter species. We accomplish this by generating the parameter species of opposing parity from the gradient species via rational multiplication CRN as shown in (24). Note that in this formulation, the annihilation reactions assumed to be present between the species of opposing parities simulate the self-subtraction of the parameter species.

$$\eta_q G_{ij}^\mp \rightarrow \eta_p P_{ij}^\pm \quad \eta = \frac{\eta_p}{\eta_q} \text{ with } \eta_p, \eta_q \in \mathbb{Z} \quad (24)$$

3.2 Training NeuralCRNs

Here, we will detail how the six CRNs defined above—two in the forward phase and four in the backpropagation phase—work in tandem to behave as a supervised learning system. We assume the presence of a clock circuit that transfers the control between two sequential steps at periodic intervals [45]. In each cycle, the clock signal catalytically activates the reaction pathways that are supposed to run in that cycle.

Fig 2 shows the detailed schematic of the training process for a single training round, illustrating the CRNs involved and the computation flow in each stage. Two distinct timelines are defined: (i) absolute timeline—to specify the order in which different stages are run; and (ii) relative timeline—to specify how long each stage runs. The stages are indicated at the top of each panel in the figure. The two signals with ‘rising’ and ‘falling’ edges at the top right of the first and third panels represent the clock triggers that transfer control to the next step. The CRNs in the second and fourth panels are assumed to run significantly faster than the CRNs in the first and third panels, thus forgoing the need for additional clock cycles at the end of these stages. This time-scale separation is based on the assumption that unimolecular reactions could be designed much faster than reactions with higher molecularity. Below, we will describe the different stages of the training process as depicted in the schematic.

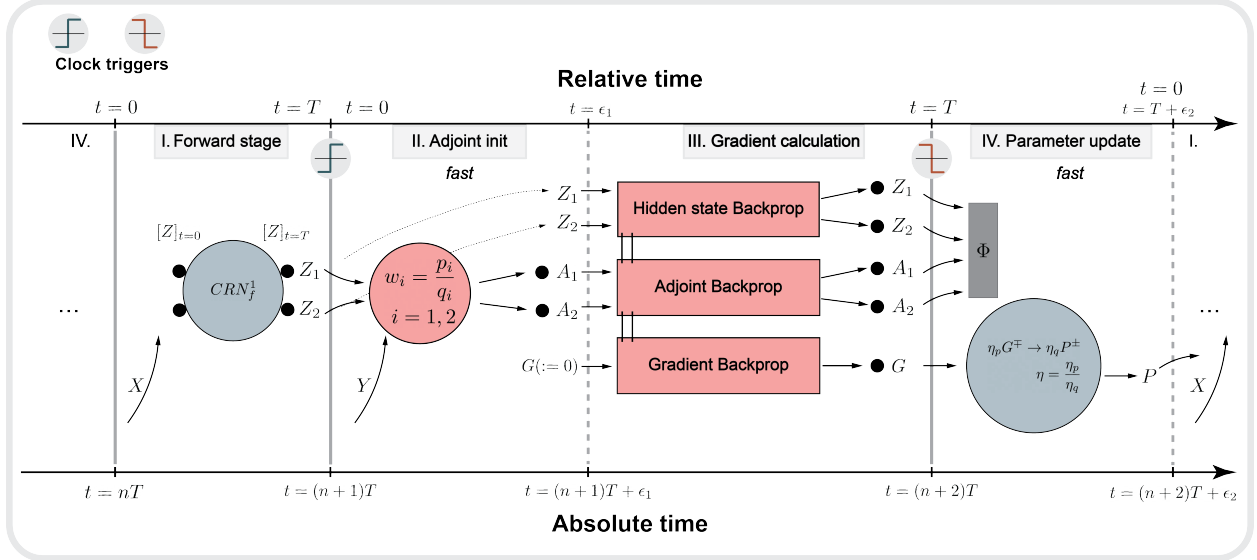


Fig 2. The training schematic of the NeuralCRNs.

The panels from left to right are considered to execute stages I, II, III, and IV of the training process. The training iteration requires two clock cycles: the ‘rising’ edge at the top right of the first panel and the ‘falling’ edge at the top right of the third panel. Time-scale separation is incorporated into the design to reduce the number of clock cycles per training stage. The panels with a ‘dashed’ line on their right boundary are considered to run significantly faster. The stages are arranged on both absolute (bottom) and relative (top) timelines. Arrows indicate the computation flow in the training procedure. Φ represents the waste species functioning as the product of degradation reactions. The parallel lines in the third panel indicate that the three backpropagation CRNs run simultaneously. (Stage I: *slow*) Runs the CRN_f^1 . It begins with the introduction of the input species X at $t = 0$, triggering the hidden state evolution until $t = T$. The clock circuit is then triggered, and the control switches to the subsequent stage. (Stage II: *fast*) Runs a merged CRN of the three CRNs CRN_f^2 , CRN_b^1 , and CRN_b^2 aimed at directly calculating the adjoint species A , skipping the intermediate steps. Time-scale separation could be enforced under certain conditions making it run quickly ($t = 0$ to $t = \epsilon_1$). (Stage III: *slow*) Runs the CRN_b^3 modeling the evolution of the gradient species G and its dependent species Z and A . The G species start from an initial zero concentration and evolve till $t = T$. The clock circuit is once again triggered, switching the control to the next stage. (Stage IV: *fast*) Runs CRN_b^4 and the degradation of the non-parametric species. Again the time-scale separation could be enforced under certain conditions to make this stage run quickly ($t = 0$ to $t = \epsilon_2$).

Stage-I. This stage involves the evolution of the hidden state species Z , i.e., running CRN_f^1 from $t = 0$ to $t = T$. The training iteration begins with the introduction of the input species X , which are also copied into Z species at $t = 0$. The evolution of Z species progresses until $t = T$, at which point the clock circuit triggers stopping this stage and switching the control to the next stage.

Stage-II (*fast*). The goal of this stage is to create the adjoint species. We observe that the three CRNs after CRN_f^1 , viz., the CRN for creating the output species CRN_f^2 , the CRN for creating the error species CRN_b^1 , and the CRN for creating the adjoint species CRN_b^2 , could be merged effectively into a single CRN as follows:

$$\begin{aligned} \hat{y} &= w_1 z_1 + w_2 z_2 && \text{from } CRN_f^2 \\ e &= w_1 z_1 + w_2 z_2 - y && \text{from } CRN_b^1 \\ a_i &= w_i w_1 z_1 + w_i w_2 z_2 - w_i y && \text{instead of } CRN_b^2 \end{aligned} \quad (25)$$

$$\begin{cases} q'_{ij} Z_j^\pm \rightarrow p'_{ij} A_i^\pm \\ q_i Y^\mp \rightarrow p_i A_i^\pm \end{cases} \quad p'_{ij} = \frac{p_i p_j}{\text{gcd}(p_i p_j, q_i q_j)}, q'_{ij} = \frac{q_i q_j}{\text{gcd}(p_i p_j, q_i q_j)}, w_i = \frac{p_i}{q_i}, w_j = \frac{p_j}{q_j} \quad \text{with } i, j = \{1, 2\}. \quad (26)$$

The expression for the adjoint in (25) is a combination of three rational multiplications (assuming that the w_i 's are rational) that can be realized using rational multiplication CRNs as shown in (26). The new coefficients p'_{ij} and q'_{ij} represent the numerator and denominator of the simplified form of the rational multiplication between w_i and w_j and gcd represents the greatest common divisor function. Note that the backpropagation

CRNs corresponding to CRN_b^3 require the A species to be fully formed before they can be run. Therefore this stage should involve an additional clock cycle. Here, we show that this requirement could be relaxed under certain assumptions.

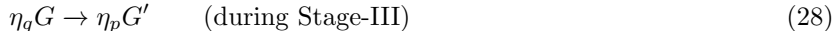
Note that we considered the final layer weights w_i to be constant. Here, we set them to 1. This effectively reduces the computation of a_i in (25) to addition and subtraction operations and the corresponding CRNs in (26) to be unimolecular, which are designed to be fast and assumed to finish within a time interval of length $\epsilon_1 \ll T$. We demonstrate the validity of this assumption by employing it in all our binary classification classifiers in §4. Note that, however, this trick doesn't work in the case of multi-class classification as the outputs are interpreted differently, i.e., they define class scores and thus cannot have identical weights throughout the final layer. Multi-class classification might require a different optimization strategy to avoid an additional clock cycle for this stage.

Stage-III. This stage models the evolution of the gradient species, i.e., running CRN_b^3 , starting from zero concentration at the end of the previous stage (at relative time $t = \epsilon_1$) to their final concentration at relative time $t = T$. The initial values of the adjoint species A and the hidden state species Z would be inducted from the end of the previous stage. At $t = T$, the clock circuit triggers, stopping the gradient evolution and switching control to the next stage.

Stage-IV (fast). This stage mainly accomplishes two tasks: (i) the updation of the parameter species P , and (ii) the degradation of the non-parametric species Z, A, X . We utilize CRN_b^4 for the first task and degradation reactions as shown in (27) for the second task.



Since the parameter update reactions in CRN_b^4 should happen before the next training round, this stage, too, requires an additional clock cycle. Here, we show how we can avoid it under certain assumptions. The degradation reactions are already unimolecular and are, therefore, fast. We suggest two ways to make the update reactions fast. The first is to set the learning rate to 1, so that $\eta_q = 1$ and the update reactions become unimolecular. Such a high learning rate might, in some cases, cause instability during training, causing the loss to diverge. In such cases, we could coerce the reactions (or add additional reactions) in Stage-III to create gradient species with a concentration equal to ηg , where g represents the expected gradient. Here, we represent the reduced concentration gradient species with G' . The parameter update can then be achieved through unimolecular reactions involving G' instead of G species. The equivalent CRNs are shown below:



Another alternative would be to reduce the time for which the backpropagation CRNs run so that the η reduction would be naturally applied. This stage would then be complete within the time range of $\epsilon_2 \ll T$. The control then switches into the next training round, where the next input comes in, and Stage-I is run until the clock triggers again at $t = T$. In cases where we cannot apply these optimizations, Stage-IV requires the addition of an extra clock cycle.

3.3 Extending to a Nonlinear-NeuralCRN

The Linear-NeuralCRN constructed above can only approximate linear separation boundaries between classes. Often, real-world datasets contain nonlinear relationships between their inputs and classification labels. Traditional neural networks incorporate this nonlinearity by employing nonlinear activation functions in their hidden layers. While this methodology generally transfers to the NeuralODEs and NeuralCRNs, for example, by introducing nonlinearity into the dynamics function, exceptions exist. One such exception is the binary classification dataset in Fig 4a with a nonlinear separation boundary between the classes. However, computations in NeuralODEs and NeuralCRNs are inherently vector flows and cannot intersect due to the uniqueness requirement of the ODE solutions [47]. As a result, classification tasks such as the one in Fig 4 generate strained flows that are difficult to overcome in practice. Therefore, in addition to using a nonlinear dynamics function, Dupont *et al.* [47] incorporated a classical machine learning technique known as *implicit*

lifting into the NeuralODEs framework to ease the training process by generating simpler flows. In this technique, the dimensionality of the classification task is *augmented*, i.e., projected onto higher dimensions a nonlinear transformation, so that the classes become linearly separable in this space [48].

Now, we will show how the Linear-NeuralCRN can be augmented to incorporate the implicit lifting technique, converting it into a *Nonlinear-NeuralCRN*: (i) We add an extra dimension to the classification task requiring appropriate dimensionality changes for all the state variables, and (ii) We utilize a nonlinear dynamics function. The first change introduces additional species and reactions corresponding to the augmented dimension. The second change requires using a nonlinear dynamics function to model the hidden state. For this, we utilize the nonlinear ODE system (30) developed by [17] that converges to a ‘smoothed’ *ReLU* activated network at steady state as shown below:

$$\frac{dz}{dt} = h + (\theta \mathbf{x} + \beta) \odot \mathbf{z} - \mathbf{z} \odot \mathbf{z} \quad (30)$$

$$\text{Let } y = \theta \mathbf{x} + \beta \quad (31)$$

$$\lim_{t \rightarrow \infty} z_i = \frac{y + \sqrt{y^2 + 4h}}{2} \approx \text{ReLU}(y) \text{ as } h \rightarrow 0. \quad (32)$$

Here, h represents the smoothing constant, θ and β represent the parameters of the ODE system, \mathbf{x} represents the input, \mathbf{z} represents the ODE state variable, and \odot represents the element-wise (hadamard) product. Note that y in (31) represents a transformation carried out by a linear neural network, and the steady-state value of z_i (32) is equivalent to applying a ‘smoothed’ *ReLU* activation to the output of a linear network, thus mimicking the operation of a *ReLU* network.

Our Nonlinear-NeuralCRN is then constructed by utilizing the ODE system in (30) as the hidden state dynamics function $f_{\theta, \beta, h}^{nl}$:

$$f_{\theta, \beta, h}^{nl} = h + (\theta \mathbf{x} + \beta) \odot \mathbf{z} - \mathbf{z} \odot \mathbf{z} \quad (33)$$

where θ and β represent the NeuralODE parameters, \mathbf{x} represents the network input and \mathbf{z} represents the hidden state (33). The rest of the construction involving the forward and backpropagation phases follows closely with that of the Linear-NeuralCRN. We augment the 2D classification problem into 3D space. Then, we substitute $f_{\theta, \beta, h}^{nl}$ into the NeuralODEs framework to enumerate the ODEs and convert them into CRNs. Note that $f_{\theta, \beta, h}^{nl}$ was developed by [17] to implement neural networks using CRNs and thus results in chemically plausible ODEs. However, their work only demonstrates the implementation of a hard-wired neural network, whereas we extend their framework to include learning.

First, we simulate the hidden state dynamics using $f_{\theta, \beta, h}^{nl}$ as the dynamics function:

$$\frac{dz}{dt} = f_{\theta, \beta, h}^{nl} = h + (\theta \mathbf{x} + \beta) \odot \mathbf{z} - \mathbf{z} \odot \mathbf{z} \quad (34)$$

$$\frac{dz_i}{dt} = h + (\theta \mathbf{x} + \beta)_i z_i - z_i^2 \quad i \in \{1, 2, 3\} \quad (35)$$

$$\frac{dz_i}{dt} = h + \sum_{i, j} \theta_{ij} x_j z_i + \beta_i z_i - z_i^2 \quad i, j \in \{1, 2, 3\} \quad (36)$$

$$\text{CRN} := \begin{cases} h & H^\pm \rightarrow Z_i^\pm \\ \theta_{ij} x_j z_j & P_{ij}^{p_\theta} + X_j^{p_x} + Z_i^{p_z} \rightarrow Z_i^{p_\theta p_x p_z} + P_{ij}^{p_\theta} + X_j^{p_x} + Z_i^{p_z} \\ \beta_i z_i & B_i^{p_\beta} + Z_i^{p_z} \rightarrow Z_i^{p_\beta p_z} + B_i^{p_\beta} + Z_i^{p_z} \\ -z_i^2 & 2Z_i^\pm \rightarrow \Phi \quad (\text{provided } Z_i^+ + Z_i^- \xrightarrow{\text{fast}} \Phi) \end{cases} \quad (37)$$

where h is the smoothing hyperparameter, x_j represent the input components with x_3 being the augmented dimension. Eq. (37) represents the CRN for the forward phase. The p_* in the species’ superscript represents the species’ dual-rail parities, and the presence of multiple parities on a species represents parity multiplication.

Similarly, the CRNs of the backpropagation phase are obtained through a similar process as follows:

$$\frac{dz_i}{dt} = -\frac{dz_i}{dt} = -h - \theta_{i1}x_1z_i - \theta_{i2}x_2z_i - \theta_{i3}x_3z_i - \beta_iz_i + z_i^2 \quad (38)$$

$$\frac{d\mathbf{a}(t)}{dt} = -\mathbf{a}(t)^T \frac{\partial f}{\partial \mathbf{z}} = - \begin{bmatrix} a_1\theta_{11}x_1 + a_1\theta_{12}x_2 + a_1\theta_{13}x_3 - 2a_1z_1 \\ a_2\theta_{21}x_1 + a_2\theta_{22}x_2 + a_2\theta_{23}x_3 - 2a_2z_2 \\ a_3\theta_{31}x_1 + a_3\theta_{32}x_2 + a_3\theta_{33}x_3 - 2a_3z_3 \end{bmatrix} \quad (39)$$

$$\frac{d}{dt} \frac{\partial \mathcal{L}}{\partial \theta} = -\mathbf{a}(t)^T \frac{\partial f}{\partial \theta} = - \begin{bmatrix} a_1x_1z_1 & a_1x_2z_1 & a_1x_3z_1 \\ a_2x_1z_1 & a_2x_2z_2 & a_3x_2z_2 \\ a_3x_1z_1 & a_3x_2z_2 & a_3x_3z_3 \end{bmatrix} \quad (\text{Note: matrix reshaped for clarity}) \quad (40)$$

$$\frac{d}{dt} \frac{\partial \mathcal{L}}{\partial \beta} = -\mathbf{a}(t)^T \frac{\partial f}{\partial \beta} = - [a_1z_1 \quad a_2z_2 \quad a_3z_3] \quad (41)$$

Note that x_i here are the inputs and are thus constant. Observe that the monomials in the ODEs contain three factor variables instead of two, as in the prior case. This implies that the corresponding CRN reactions would be trimolecular, which increases the implementation complexity. The ODE to CRN translation follows a similar procedure illustrated in the template construction but with the presence of an extra variable. Note that the signs of the backpropagation ODEs (39) and (41) and (40) have to be inverted before converting them into CRNs. For the sake of conciseness, we delegate the CRNs of these ODEs to SI text S3.

4 Results

In this section, we validate our constructions by showing that they can successfully learn binary classification datasets with linear (with Linear-NeuralCRN) and nonlinear (with Nonlinear-NeuralCRN) separation boundaries. Later, we will show that this binary classification framework can be easily extended to a multi-class framework and demonstrate this on two real-world multi-class datasets. Below, we refer to the class with ‘1’ as the *positive* class and the class with label ‘0’ as the *negative* class.

4.1 Linear dataset

Linear is a synthetic two-dimensional binary classification dataset with linearly separable classes (Fig 3a). Each data point $\mathbf{x} := (x_1, x_2)$ in the dataset is created by sampling randomly from the normal distribution $\mathcal{N}(0, 1)$. The class label y is assigned by comparing the weighted sum of the input components with a predefined threshold Th :

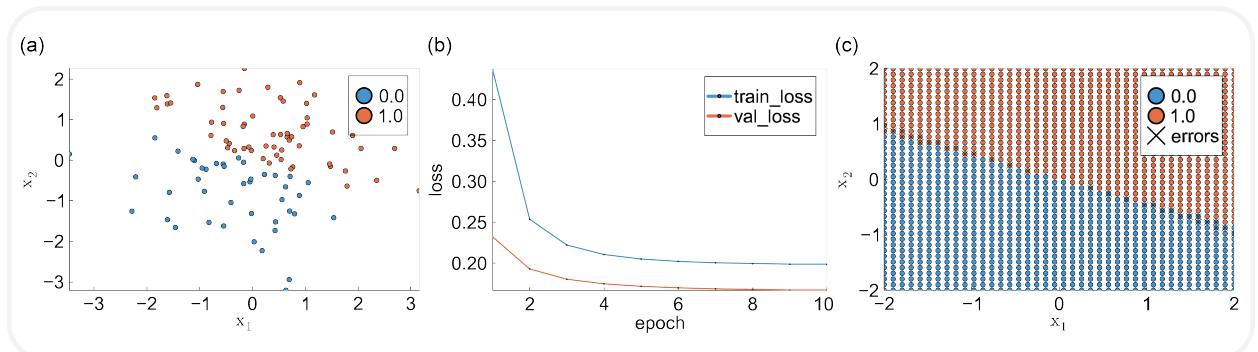


Fig 3. (a) Training set of the *Linear* dataset. The discriminant function is $g(x_1, x_2) = x_1 + 2x_2$ with classes assigned ‘1’ or ‘0’ depending on whether the value of g is above or below a threshold (here, 0.0). (b) Training and validation loss plots show the loss convergence. (c) The labels assigned by the trained model on the validation set with the misclassified samples marked with an \times .

$$y = \begin{cases} 1, & \text{if } c_1x_1 + c_2x_2 > Th \\ 0, & \text{otherwise.} \end{cases}$$

where the coefficient values and the threshold are set as follows: $c_1 = 1.0, c_2 = 2.0$, and $Th = 0$. Briefly, a data point is assigned to the positive class if the weighted sum exceeds the threshold and to the negative class otherwise.

We use the Linear-NeuralCRN for this task. The training and the validation sets are created with 100 samples each, equally distributed among the two classes. The test set is created as a 2D grid with uniformly spaced points to allow for the visualization of the separation boundary learned by the model. The parameter species P_{ij} are initialized through Xavier initialization ([49]; also see SI text S1). Recall that the final classification layer weights w_1 and w_2 are considered to be constant and are initialized to 1. We provide a full description of our parameter choices in SI text S1.

Fig 3b depicts the loss curves, showing that the training loss has converged, closely followed by the validation loss curve, indicating that our model has learned the underlying data distribution. Fig 3c depicts the predictions on the test set, which show the separation boundary and the misclassified examples (marked by an \times). The intercepts at the plot boundary (left: $x_1 = -2, x_2 \approx 1$ and right: $x_1 = 2, x_2 \approx -1$) satisfying $x_1 + 2x_2 = 0$ are further proof that our Linear-NeuralCRN model correctly learned the underlying data distribution. Finally, we show that the parameter trajectories of our model during training match closely with those of an equivalent NeuralODE, starting from identical parameters, further bolstering the validity of our construction and the training process (see SI text S5).

4.2 Rings dataset

Rings is a 2D binary classification dataset with nonlinearly separable classes arranged into two concentric rings of different radii ranges centered at the origin (Fig 4a). The data points $\mathbf{x} = (x_1, x_2)$ are created by independently sampling from the uniform distribution $\mathcal{U}(-1, 1)$. The classification label y for each \mathbf{x} is assigned using three radii parameters $r_1, r_2, r_3 \in \mathbb{R}_{>0}$ satisfying $r_1 < r_2 < r_3$ as follows:

$$y = \begin{cases} 0, & \text{if } 0 < \|\mathbf{x}\|_2 < r_1 \\ 1, & \text{if } r_2 < \|\mathbf{x}\|_2 < r_3 \end{cases}$$

Briefly, the data points in the inner ring, i.e., within a distance of r_1 from the origin, are assigned to the negative class, and the data points within a distance range of (r_2, r_3) are assigned to the positive class. The values of r_1, r_2 , and r_3 are arbitrarily chosen as follows: $r_1 = 0.4, r_2 = 0.6$, and $r_3 = 1$.

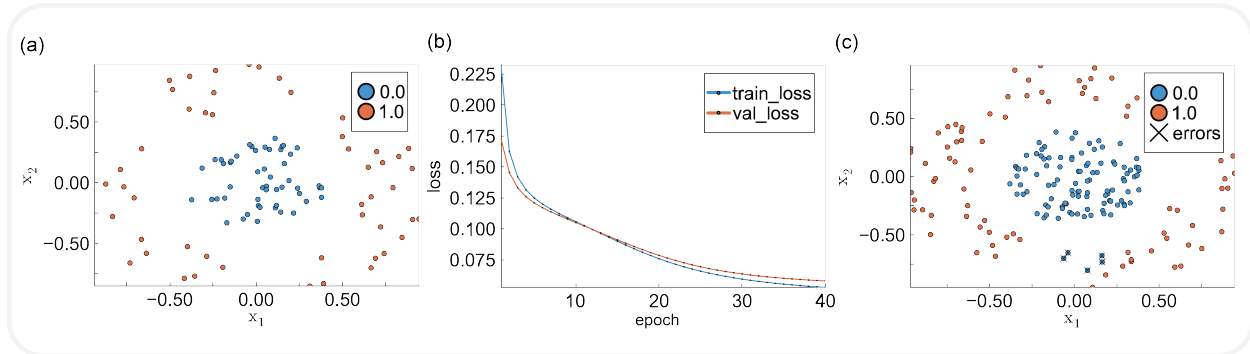


Fig 4. Modeling binary classification in the NeuralCRNs framework.

(a) The training set of the *Rings* dataset. (b) Training and validation loss plots showing the loss convergence. (c) The labels assigned by the trained model on the validation set with misclassified samples marked with an \times .

We train the Nonlinear-NeuralCRN on this dataset. As discussed before, we augment the dimensionality converting it into a 3D classification task. The parameter initialization follows a similar procedure to that of the ‘Linear’ dataset. The training and validation sets consist of 100 samples each, equally distributed between the two classes (Fig 4a). There is no test set for this task, and the validation set itself acts as the test set. Note that the validation set is not used in model training, despite its name, as we do not perform any hyperparameter tuning. Fig 4b shows the convergence of the loss curves for both the training and validation sets. Fig 4c shows the predictions made by the trained model on the validation set with the misclassified samples marked with an \times . The model attains an accuracy of about 0.98 on the validation set, indicating

that our Nonlinear-NeuralCRN can learn nonlinear separation boundaries. Fig S2 illustrates the implicit lifting by the trained Nonlinear-NeuralCRN model performed on the validation dataset where nonlinearly separable classes in 2D evolved to be linearly separable in 3D space.

4.3 XOR, AND, and OR datasets

We further test the learning capabilities of our Nonlinear-NeuralCRN on nonlinear classification tasks with separation boundaries defined by boolean functions XOR, AND, and OR. The corresponding datasets are named *XOR*, *AND*, and *OR*. Note that we use verbatim format to represent the boolean functions (e.g., XOR) and italics to represent the corresponding dataset (e.g., *XOR*). We refer to them collectively as the *Boolean datasets*.

These datasets are created as follows. The data points $\mathbf{x} = (x_1, x_2)$ are independently sampled from the uniform distribution $\mathcal{U}(0.0, 1.0)$. The class labels are assigned by first transforming the real-valued variables x_i into their boolean form x_i^b and applying the Boolean function to them (43). Conversion to the boolean form is accomplished by comparing the variable to a predefined threshold Th as shown in (42).

$$x_i^b = \begin{cases} 1 & \text{if } x_i > Th \\ 0 & \text{otherwise} \end{cases} \quad i = 1, 2 \quad (42)$$

$$y = F(x_1^b, x_2^b) \quad F \in \{\text{XOR, AND, OR}\}. \quad (43)$$

Fig 5 shows the training sets of the three boolean datasets. Briefly, the *XOR* dataset is positive only in the second and fourth quadrants, *AND* dataset is positive only in the first quadrant, and *OR* is positive in the first, second, and fourth quadrants. Note that the quadrants here are mentioned in a relative sense by considering $(0.5, 0.5)$ as the origin.

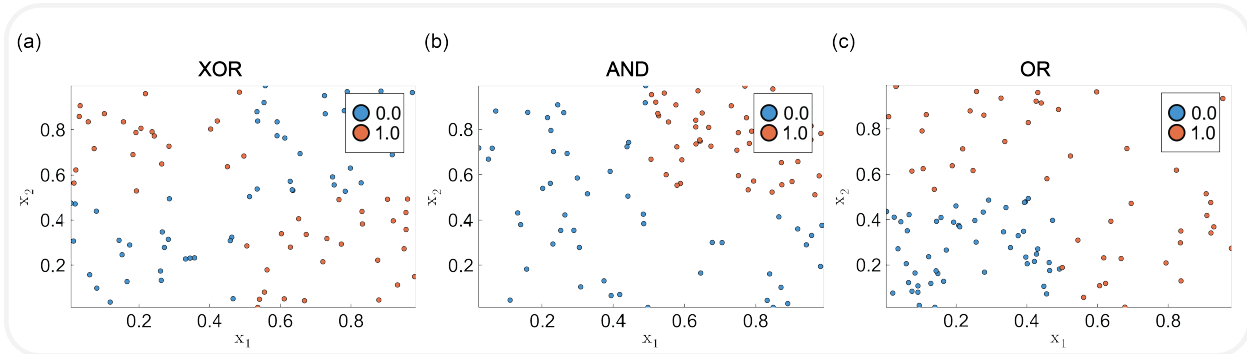


Fig 5. Training Nonlinear-NeuralCRN on the Boolean datasets.

Training sets of the Boolean datasets (a) *XOR*, (b) *AND*, and (c) *OR*. Each dataset contains 100 samples each, equally distributed among the positive and negative classes. The sampled data points are first converted into their boolean format by comparing them with a threshold, and the corresponding boolean function is applied to obtain the class label.

The Nonlinear-NeuralCRN is trained on each of these datasets in an augmented 3D space. Fig 6 shows the rough separation boundaries learned by the model on a uniformly spaced grid of test data points for the models trained on *XOR*, *AND*, and *OR* datasets. Note that the separation boundaries, while being qualitatively sound, do not exactly mimic the expected separation boundaries. This is because the datasets are deliberately kept sparse to minimize the number of training rounds in the chemical implementation. The primary goal is not to simulate the boundaries of the boolean functions but to demonstrate that our model can simulate nonlinear separation boundaries. Further, we note that while augmenting the NeuralCRN to model nonlinear functions is not always required, we do so for the sake of consistency. For example, we show the results of training a 2D Nonlinear-NeuralCRN without augmenting on the *OR* dataset in SI text S4.

4.4 Multiclass classification

So far, we have only dealt with NeuralCRN architectures for binary classification. Now we will show how the previous architectures can be modified to support multi-class classification. First, we identify that the only

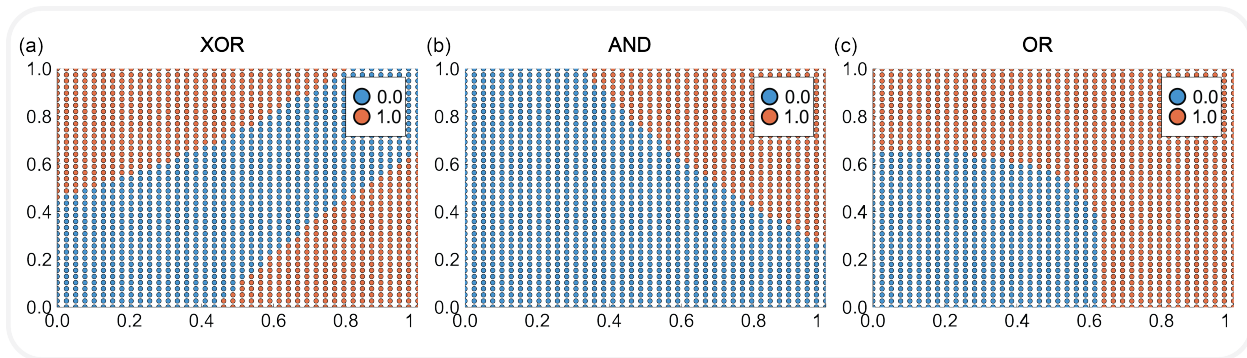


Fig 6. Decision boundaries learned by Nonlinear-NeuralCRN on Boolean datasets.

Predictions on a test grid showing the decision boundaries formed by the Nonlinear-NeuralCRN trained on (a) *XOR*, (b) *AND*, and (c) *OR* datasets.

difference between the two is the way the output is read out. The binary classification model employs the logistic regression formulation, where a single scalar output is interpreted as the class label by comparing it with a threshold. In contrast, the outputs of multi-class classification represent the individual class scores, with the highest-scoring class acting as the class label. The class labels are represented using *one-hot* encoding, i.e., as a binary vector with only one component in the ON state (as ‘1’) and the rest in the OFF state (as ‘0’). Consequently, the extension to multi-class classification could be easily performed by replacing the final layer in the prior architectures with a fully connected layer, with the size of output nodes equal to the class cardinality. No changes are required to core NeuralCRN architecture, except for adjusting to the dimensionality of the classification task. We now validate our construction for multi-class classification using two real-world datasets: (i) the Iris dataset [50] and (ii) the Virus Infection dataset [51].

Iris. The *Iris* dataset consists of the measurements of the width and length dimensions of the petal and sepal corresponding to the flowers of three different species in the *Iris* genus, namely *Iris-setosa*, *Iris-virginica*, and *Iris-versicolor*. It is a four-input dataset containing a total of 150 sample measurements divided equally among the three species, with each data point containing 4 real-valued features.

Virus Infection. The *Virus Infection* dataset is a small part of a larger collection NCBI GSE73032 [52] with gene expression data of 12023 genes collected through micro-array assays from live human subjects. The subjects are inoculated separately with four respiratory viruses, viz., H1N1, H3N1, HRV, and RSV, and the gene expression values are measured at several time points before, during, and after inoculation. However, we only utilize a small subset of this dataset following the procedure suggested by [20]. Specifically, we collect gene expression data only at the disease *onset time*—the time point at which symptoms appear. Then, we utilize a random forest (RF) classifier (from Scikit-learn python package [53]) to select the top 9 genes from 12023, according to the feature importance scores provided by the RF classifier. The resultant dataset comprises 550 data points distributed unequally among the four classes.

For both the tasks (Iris and Virus Infection), the training set is constructed by randomly sampling 90% of the data points from each class, while the rest are put into the test set. Then, the training sets are subjected to min-max normalization, and the normalizing factors derived from the training set are used to normalize the test set. The Nonlinear-NeuralCRN is trained in 5D augmented space for Iris (four features and one augmented dimension) and 10D augmented space for Virus Infection tasks (nine features and one augmented dimension). Fig 7 shows the NeuralCRN architectures, validation accuracies at different stages of training, and inference schematic for the Iris and Virus Infection tasks, respectively. In both tasks, the trained model achieved an accuracy close to 1, indicating that our Nonlinear-NeuralCRN model can perform multi-class classification with nonlinearly separable classes.

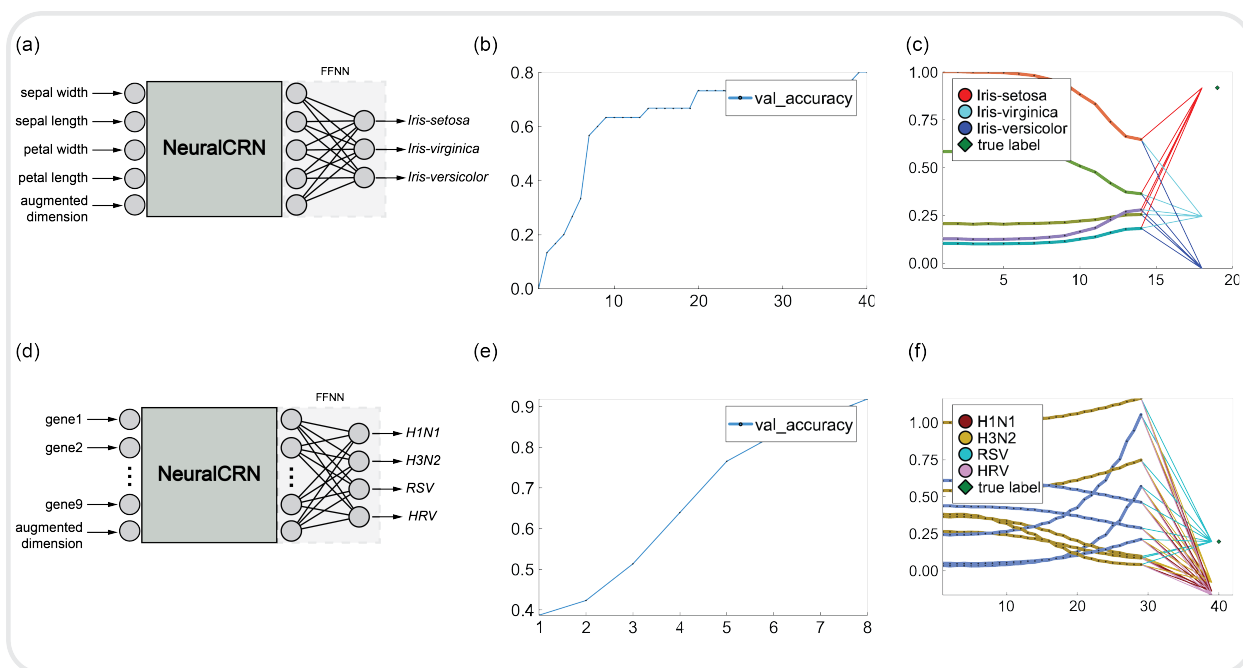


Fig 7. Modeling multi-class classification in the NeuralCRNs framework.

(a)-(c) correspond to the *Iris* dataset and (d)-(f) correspond to the *Virus Infection* dataset. (a, d) The NeuralCRN architectures for training on the *Iris* and *Virus Infection*, respectively. It shows the input features and the class labels. The architecture differs from that of the binary classification architecture in that the outputs correspond to the class scores assigned by the model. The highest-scoring class is chosen as the prediction label. (b, e) Accuracy on the validation set as the training proceeds. The accuracy reaches close to 1, indicating that the training was successful. (c, f) Illustrations of the prediction process showing the NeuralCRN “vector” flows (curved lines) and the weighted sum calculation at the classification layer (straight lines).

5 Discussion

In this work, we presented NeuralCRNs, a deterministic chemical reaction system capable of autonomous neural network-like learning in the chemical medium. Instead of mimicking the functionality of conventional feedforward neural networks (FFNNs) in the chemical medium [15, 20, 21, 27, 28, 30] (henceforth referred to as *CheFFNNs*), the NeuralCRNs framework is founded upon dynamical system-based continuous-time neural networks. Specifically, our framework is derived from the NeuralODEs framework, where the neural computations are modeled as ODEs. The novelty of our work lies in combining the theory of NeuralODEs [35] with CRN theory [37, 54] and stitching them together into a supervised learning framework. We also presented several optimizations to the framework to simplify it for a future physical implementation.

We instantiated two different supervised learning classifiers for binary classification using the NeuralCRNs framework: Linear-NeuralCRN for linear classification and Nonlinear-NeuralCRN for nonlinear classification. We then validated our constructions by training and evaluating them on datasets with both linearly separable and nonlinearly separable classes. We further tested their performance on “Boolean” datasets, including *XOR*, *AND*, and *OR*, demonstrating that the framework can effectively approximate nonlinear decision boundaries. Finally, we showed that the binary classification framework could be extended to support multi-class classification by simply modifying the final classification layer and demonstrating its validity on two real-world datasets.

Comparing NeuralODEs and NeuralCRNs. Theoretically, NeuralCRNs could be considered equivalent to the NeuralODEs. However, NeuralCRNs have more aggressive physical limitations. For example, conventionally, NeuralODEs utilize FFNNs to model their dynamics (f_θ), to exploit the parallelism offered by GPUs and TPUs [55], as well as the convenient calculation of $\frac{\partial f}{\partial \theta}$ through automatic differentiation [36]. In contrast, the choice of f_θ is restricted to the functions that can generate lower-order polynomial ODE systems that provide uniqueness guarantees viz., differentiable and Lipschitz continuous (mass action ODE systems) [17].

The use of a clock circuit. A key aspect of the NeuralCRNs framework is implementing isolation between

different sequential stages, for example, between the forward and backpropagation phases. We assume the presence of a “sequencer” or a “clock” circuit that oversees the control transfer between the current stage and the next. It is suggested previously [45] that such a clock circuit could be implemented through a chemical oscillator system [9,10], where the dominant signal in each oscillator cycle can conditionally enable and disable reaction pathways. A potential strategy to achieve such conditional execution in chemical circuits is through activation and inhibition reactions, for example, as demonstrated in “buffered” DNA strand displacement gates architecture [15] or in the spiking neuron architecture of [34]. However, a chemical oscillator is a non-equilibrium system comprising autocatalytic reactions [30,45] that are specifically hard to implement in practice due to leakage errors that amplify nonlinearly. Therefore, it is crucial to minimize the influence of the clock circuit in the circuit execution. In this work, we have presented several optimizations to the training procedure that practically cut down the number of clock cycles per training iteration to 2.

The CRNs of the NeuralCRNs framework. The CRNs in the NeuralCRNs framework are rate-independent [56]. For simplicity, we consider the reactions to have a unit rate constant unless explicitly specified. Here, we slightly abuse the notation by setting the rate constants of both the bimolecular and trimolecular reactions to $k = 1.0$, despite the difference in the units. The time interval for which the system runs is not too critical, provided that both the forward and backpropagation phases run for a similar (if not for an identical) amount of time. The reactions are noncompetitive [20] in that the reactions are catalytic in the reactants as previously utilized by [43] and [42]. Further, the chemical species and, thus, the reactions are specified in the dual-rail format. Since the circuit involves autocatalytic reactions, fast annihilation reactions (as specified in [57] for example) are enabled between the complementary dual-rail species to prevent the concentrations from exploding. Finally, unimolecular reactions are considered to be significantly faster (on a similar time scale as the annihilation reactions) compared to the reactions of higher molecularity (bimolecular and trimolecular reactions).

Comparing NeuralCRNs and CheFFNN frameworks. How does the implementation complexity of the NeuralCRNs framework compare to an analogous CheFFNN? We provide two comparisons using the examples of (i) a perceptron linear classifier and (ii) a nonlinear ‘ReLU’ network. For the perceptron linear classifier, we choose the *Analog Asymmetric Signal Perceptron* (AASP) model from [28] to approximate linear functions of the form $y = k_0 + k_1x_1 + k_2x_2$, where k_0, k_1, k_2 are the function coefficients. Their original circuit consists of 17 species and 18 reactions. However, for the sake of simplicity, we remove the bias term k_0 , which results in a circuit of 14 species and 14 reactions. We implement an analogous minimal NeuralCRN circuit in SI text S2 using $f_\theta(\mathbf{x}) = \theta \odot \mathbf{x}$. The resulting circuit consisted of 12 species and 11 reactions. Note that both circuits represent only positive-valued functions, although certain species in the NeuralCRNs framework should be specified in the dual-rail format. While the two circuits are similar in terms of the circuit size, their main difference emanates from the nature of their underlying reactions. For instance, the reactions of AASP are enzymatic, requiring controlled conditions of temperature and pH and enforcing strict constraints on the rate constant values. In contrast, the NeuralCRN reactions are enzyme-free and could thus be operated at room temperature. Also, the reaction rates are unconstrained, provided that the reaction runs for a sufficient amount of time.

The difference is more conspicuous in the case of nonlinear classification. Here, we compare our Nonlinear-NeuralCRN with two different CheFFNN implementations, each representing a different flavor of CheFFNN computations: (i) a non-competitive CRN-based ReLU network (NC-ReLU) [20] and (ii) a hyperbolic tangent (*Tanh*) activated network that uses weight perturbation algorithm for learning (WP-Tanh) [30]. They both are two-input three-layer networks that use *ReLU* and *Tanh* as the hidden (middle) layer activation functions, respectively. To draw an analogy, the final hidden state after CRN_f^1 in NeuralCRNs could be analogized to the hidden state activations in the CheFFNNs. In what follows, we assume a hybrid CheFFNN implementation, borrowing, in part, the ideas from both the above networks. The NC-ReLU utilizes non-competitive CRNs for its computations, which are also used in our NeuralCRNs construction. However, the presence of the *ReLU* (or any other nonlinear) activation in the hidden layer requires that the input weighted-sum species ($\text{crn_mult}(X, W)$) are fully formed at the hidden layer before the CRNs for computing the activation function are enabled. This implies that the presence of a nonlinear activation function induces an additional clock cycle into the network. Note that the NC-ReLU framework was only specified for the forward stage in its source work [20]. On the other hand, the WP-Tanh network adopts an alternative approach, where the

computations are spread out over multiple clock cycles to simplify the CRNs. Learning is performed using the weight perturbation algorithm as follows: (a) an identical “shadow” circuit [58] is installed alongside the main circuit; (b) a single weight w_i is perturbed in each round (by Δw_i) in the shadow circuit $w_i + \Delta w_i$, and the relative loss difference with respect to this perturbation is used to approximate the parameter gradients as shown in (44).

$$\frac{\partial \mathcal{L}}{\partial w_i} \approx \frac{\mathcal{L}(w_i + \Delta w_i) - \mathcal{L}(w_i)}{\Delta w_i} \quad (44)$$

The process is repeated for each weight in successive clock cycles. In contrast, the NeuralCRNs framework calculates all the gradients in a single clock cycle. Another drawback of the weight perturbation algorithm (also mentioned by the authors in [30]) is that the individual weight updates do not necessarily move the loss curve towards convergence (either oscillates or gets stuck in local minima), thus requiring a large number of training rounds. The authors also suggest changes to their weight perturbation algorithm to update all the weights collectively, but this involves a significant increase in the circuit size. In contrast, our architecture provides theoretical guarantees for loss convergence [17]. Finally, the weight perturbation algorithm calculates a first-order approximation of gradients, which could result in compounding errors when the circuit is scaled up, whereas the NeuralCRNs backpropagation methodology estimates precise gradients.

Towards a biochemical implementation of NeuralCRN. One possible way to experimentally realize our NeuralCRN constructions could be through DNA-based reaction systems. DNA is an excellent substrate for modeling chemical behavior, owing to the specificity of its base-pair interactions, resulting in programmable reaction pathways. Indeed, several “learning” CRNs have already been implemented in DNA-based synthetic chemistries [15,21,31]. Of particular importance is a specific reaction motif known as DNA strand displacement (DSD) [59,60], which was shown to be capable of emulating arbitrary chemical reaction systems [19]. In addition, the DSD framework is simple, modular, and flexible, which eases the complexity of circuit design. Furthermore, these reactions could be catalyzed by enzymes [61,62] or run in an enzyme-free mode, thus providing functional flexibility [9,63–66].

However, several challenges must be addressed before we can reliably obtain a DNA-based implementation of NeuralCRNs. While DSD circuits can, in theory, simulate arbitrary chemical reaction systems [19], in practice, they have several issues, such as: (a) cross-talk due to limited oligonucleotide design space [67], (b) slow reactions [68], and (c) “leakage” errors (or leaks) [60,68] which occur due to nonspecific interactions between the substrates. Leakage errors, especially in circuits with complex behaviors, cause a significant hindrance to scaling up the DSD circuits [10,58] as the leaked strands interact with the downstream circuit, rapidly degrading the circuit behavior. However, these ill effects could be partially mitigated by enforcing certain “leakless” design constraints [69,70]. A future DNA implementation of NeuralCRNs might involve adaptive circuit elements such as “buffered” DSD gates [15], spiking neuron-like systems [34], DNA-based temporal [71], time-delay [72], and timer [73] circuits.

Time-scale separation. Recall that in our NeuralCRN construction, we assume that some reactions (specifically, adjoint species initialization in CRN_b^1 and parameter update in CRN_b^3) are designed to run faster than the rest to reduce the circuit complexity by reducing the number of clock cycles required per training iteration. We draw attention to the fact that these reactions are unimolecular (under certain assumptions). The time-scale separation then comes naturally as DSD implementations of unimolecular reactions could be achieved through a single strand displacement reaction, whereas reactions of higher molecularity require multiple cascaded reactions [19,62]. This rate divide could be further enhanced by scaling up the unimolecular circuit and scaling down the bimolecular and trimolecular circuits.

The issue with the dual-rail notation. Another obstacle towards a physical implementation of NeuralCRNs is its reliance on the dual-rail encoding, which significantly bloats up the circuit size. For example, the number of reactions in Linear-NeuralCRN increases by $4\times$ (two variable monomials) and by $8\times$ in the Nonlinear-NeuralCRN (three variable monomials). Typically, in DSD implementations, each abstract reaction translates into two reactions and requires creating at least two new “gate” complexes [10,19,74]. Thus, instead of just two new species, a dual-rail implementation in Nonlinear-NeuralCRN would now require the creation of 16 new species. However, most of the reactions wouldn’t be active due to the presence of annihilation reactions between the complementary dual-rail species. Nevertheless, the circuit requires the corresponding

species to be present in the system. Several methodologies have been suggested to avoid dual-rail notation, for example, by setting a threshold for each species such that values above it are considered positive and values below it are considered negative [28]. However, such methodologies only apply in limited contexts, and reducing the circuit size is an open problem.

Future work. Possible extensions to the NeuralCRNs framework could include using other activation functions that satisfy the requirements, such as the hyperbolic tangent [30]. An interesting offshoot of our work would be constructing learning CRNs using stochastic differential equations, analogous to the framework described in [55]. Such a framework could allow for learning in stochastic environments that are non-well-mixed reaction networks (e.g., the cell). Learning CRNs based on probabilistic models such as Boltzmann machines [75] and hidden markov models [76] have already been proposed.

Converting the parameter values into CRN concentrations is an important problem that this work did not address. One potential way to ensure that the parameter variance is within the range for a DNA implementation is by carefully choosing the initial parameter values and enforcing gradient *clipping* (restricting them to a maximum absolute value) [77]. For reference, the concentration range for DSD circuits could range from $1 - 10^4$ nM [19]. However, the higher concentration ranges are reserved for the fuel species, whereas the abstract CRN species are typically modeled as the signal strands, which are typically limited to the lower concentration range.

Potential applications of adaptive molecular systems. The biocompatibility of DNA and the adaptive capabilities of NeuralCRNs could usher in de novo molecular machines that can autonomously sense and manipulate the biochemical environments they are deployed in. The most promising application of such capabilities seems to be in the field of *in vivo* nanomedicine [21]. Of particular interest are DNA-based computational circuits embedded within DNA origami-based vesicles enabling molecular-scale diagnostic [78,79] and therapeutic systems [80,81] with adaptive capabilities to tackle dynamically changing environments [82] or host behaviors [21]. They could train and augment the immune system against the threat of continuously evolving virus genomes [21,83]. Furthermore, they could be the decision-making organs of artificial cells fabricated using biomolecules [84,85].

6 Methods

All the simulations were performed in Julia using the `Catalyst.jl` package, with numerical solver `TRBDF2()`. We set the relative tolerance to 10^{-4} , absolute tolerance to 10^{-6} , and the maxiters to 10^6 (values are chosen by trial and error). For faster experimentation, we implemented a tool to generate the CRNs of NeuralCRNs by simply specifying the ODEs in their vector form. The code for this tool can be found here [Code].

7 Conclusion

We presented NeuralCRNs, a chemically natural implementation of learning in chemical reaction systems. In this implementation, computations are realized by simple concentration readouts at predefined intervals. Our implementation thus eliminates the nonidealities that crop up in chemical implementations of digital computations. Further, the classifiers constructed only use unimolecular, bimolecular, and trimolecular reactions, making them chemically plausible. We then presented several optimizations to the constructed framework and discussed several impediments towards its physical realization, setting up future theoretical and experimental work. Thus, we believe our work is a positive step towards constructing adaptive molecular systems that could function effectively in uncertain biological environments.

References

1. Koshland DE Jr. Special essay. The seven pillars of life. *Science*. 2002;295(5563):2215–2216.
2. Hennessey TM, Rucker WB, McDiarmid CG. Classical conditioning in paramecia. *Anim Learn Behav*. 1979;7(4):417–423.
3. Webre DJ, Wolanin PM, Stock JB. Bacterial chemotaxis. *Current Biology*. 2003;13(2):R47–R49.
4. Fernando CT, Liekens AML, Bingle LEH, Beck C, Lenser T, Stekel DJ, et al. Molecular circuits for associative learning in single-celled organisms. *J R Soc Interface*. 2009;6(34):463–469.
5. Kim J, Hopfield J, Winfree E. *Advances in Neural Information Processing Systems*. vol. 17. Saul LK, Weiss Y, Bottou L, editors. MIT Press; 2004.
6. Bray D. Protein molecules as computational elements in living cells. *Nature*. 1995;376(6538):307–312.
7. Eshra A, Shah S, Song T, Reif JH. Renewable DNA Hairpin-Based Logic Circuits. *IEEE Transactions on Nanotechnology*. 2019;18:252–259. doi:10.1109/TNANO.2019.2896189.
8. Qian L, Winfree E. A simple DNA gate motif for synthesizing large-scale circuits. *J R Soc Interface*. 2011;8(62):1281–1297.
9. Fujii T, Rondelez Y. Predator–prey molecular ecosystems. *ACS nano*. 2012;7(1):27–34.
10. Srinivas N, Parkin J, Seelig G, Winfree E, Soloveichik D. Enzyme-free nucleic acid dynamical systems. *bioRxiv*. 2017; p. 138420.
11. Oishi K, Klavins E. Biomolecular implementation of linear I/O systems. *IET Systems Biology*. 2011;5(4):252–260.
12. Yordanov B, Kim J, Petersen RL, Shudy A, Kulkarni VV, Phillips A. Computational design of nucleic acid feedback control circuits. *ACS synthetic biology*. 2014;3(8):600–616.
13. Chen YJ, Dalchau N, Srinivas N, Phillips A, Cardelli L, Soloveichik D, et al. Programmable chemical controllers made from DNA. *Nat Nanotechnol*. 2013;8(10):755–762.
14. Qian L, Winfree E, Bruck J. Neural network computation with DNA strand displacement cascades. *Nature*. 2011;475(7356):368–372.
15. Lakin MR, Stefanovic D. Supervised Learning in Adaptive DNA Strand Displacement Networks. *ACS Synth Biol*. 2016;5(8):885–897.
16. Cherry KM, Qian L. Scaling up molecular pattern recognition with DNA-based winner-take-all neural networks. *Nature*. 2018;559(7714):370–376.
17. Anderson DF, Joshi B, Deshpande A. On reaction network implementations of neural networks. *J R Soc Interface*. 2021;18(177):20210031.
18. Dalchau N, Szép G, Hernansaiz-Ballesteros R, Barnes CP, Cardelli L, Phillips A, et al. Computing with biological switches and clocks. *Natural computing*. 2018;17(4):761–779.
19. Soloveichik D, Seelig G, Winfree E. DNA as a universal substrate for chemical kinetics. *Proc Natl Acad Sci*. 2010;107(12):5393–5398.
20. Vasić M, Chalk C, Luchsinger A, Khurshid S, Soloveichik D. Programming and training rate-independent chemical reaction networks. *Proc Natl Acad Sci U S A*. 2022;119(24):e2111552119.
21. Lakin MR, Minnich A, Lane T, Stefanovic D. Design of a biochemical circuit motif for learning linear functions. *J R Soc Interface*. 2014;11(101):20140902.

22. Bedau MA. Artificial life: organization, adaptation and complexity from the bottom up. *Trends Cogn Sci*. 2003;7(11):505–512.
23. Rosenblatt F. The perceptron: a probabilistic model for information storage and organization in the brain. *Psychol Rev*. 1958;65(6):386.
24. Hinton GE. How neural networks learn from experience. *Scientific American*. 1992;267(3):144–151.
25. Rumelhart DE, Hinton GE, Williams RJ. Learning representations by back-propagating errors. *Nature*. 1986;323(6088):533–536.
26. Nagipogu RT, Fu D, Reif J. A survey on molecular-scale learning systems with relevance to DNA computing. *Nanoscale*. 2023;.
27. Banda P, Teuscher C, Lakin MR. Online learning in a chemical perceptron. *Artif Life*. 2013;19(2):195–219.
28. Banda P, Teuscher C. *International Conference on Unconventional Computation and Natural Computation*. Ibarra OH, Kari L, Kopecki S, editors. Springer; 2014.
29. Blount D, Banda P, Teuscher C, Stefanovic D. Feedforward Chemical Neural Network: An In Silico Chemical System That Learns xor. *Artif Life*. 2017;23(3):295–317.
30. Arredondo D, Lakin MR. Supervised Learning in a Multilayer, Nonlinear Chemical Neural Network. *IEEE Trans Neural Netw Learn Syst*. 2022;PP.
31. Okumura S, Gines G, Lobato-Dauzier N, Baccouche A, Deteix R, Fujii T, et al. Nonlinear decision-making with enzymatic neural networks. *Nature*. 2022;610(7932):496–501.
32. Gong L, Zhao Z, Lv YF, Huan SY, Fu T, Zhang XB, et al. DNAzyme-based biosensors and nanodevices. *Chem Commun*. 2015;51(6):979–995.
33. McCulloch WS, Pitts W. A logical calculus of the ideas immanent in nervous activity. *Bull Math Biophys*. 1943;5(4):115–133.
34. Hjelmfelt A, Weinberger ED, Ross J. Chemical implementation of neural networks and Turing machines. *Proc Natl Acad Sci*. 1991;88(24):10983–10987.
35. Chen RT, Rubanova Y, Bettencourt J, Duvenaud DK. Neural ordinary differential equations. *Advances in neural information processing systems*. 2018;31.
36. Rall LB. *Automatic differentiation: Techniques and applications*. Springer; 1981.
37. Hárs V, Tóth J. On the inverse problem of reaction kinetics. *Qualitative theory of differential equations*. 1981;30:363–379.
38. Runge C. Über die numerische Auflösung von Differentialgleichungen. *Mathematische Annalen*. 1895;46(2):167–178.
39. Kutta W. *Beitrag zur näherungsweise Integration totaler Differentialgleichungen*. Teubner; 1901.
40. Hairer E, Wanner G. Algebraically stable and implementable Runge-Kutta methods of high order. *SIAM Journal on Numerical Analysis*. 1981;18(6):1098–1108.
41. Pontryagin LS. *Mathematical Theory of Optimal Processes*. CRC Press; 1987.
42. Cardelli L, Tribastone M, Tschaikowski M. From electric circuits to chemical networks. *Nat Comput*. 2020;19(1):237–248.
43. Oishi K, Klavins E. Biomolecular implementation of linear I/O systems. *IET Syst Biol*. 2011;5(4):252–260.

44. Buisman H, ten Eikelder HM, Hilbers PA, Liekens AM. Computing algebraic functions with biochemical reaction networks. *Artificial life*. 2009;15(1):5–19.
45. Vasić M, Soloveichik D, Khurshid S. CRN++: Molecular programming language. *Natural Computing*. 2020;19:391–407.
46. Cox DR. The regression analysis of binary sequences. *Journal of the Royal Statistical Society: Series B (Methodological)*. 1958;20(2):215–232.
47. Dupont E, Doucet A, Teh YW. *Augmented Neural ODEs*; 2019.
48. Mercer J. Xvi. functions of positive and negative type, and their connection the theory of integral equations. *Philosophical transactions of the royal society of London Series A, containing papers of a mathematical or physical character*. 1909;209(441-458):415–446.
49. Glorot X, Bengio Y. Understanding the difficulty of training deep feedforward neural networks. *Proceedings of the thirteenth*. 2010;.
50. Fisher RA. *Iris*; 1988. UCI Machine Learning Repository.
51. Liu TY, Burke T, Park LP, Woods CW, Zaas AK, Ginsburg GS, et al. An individualized predictor of health and disease using paired reference and target samples. *BMC Bioinformatics*. 2016;17:47.
52. Host gene expression signatures of H1N1, H3N2, HRV, RSV virus infection in adults; 2016. Available from: <https://www.ncbi.nlm.nih.gov/geo/query/acc.cgi?acc=GSE73072>.
53. Pedregosa F, Varoquaux G, Gramfort A, Michel V, Thirion B, Grisel O, et al. Scikit-learn: Machine Learning in Python. *Journal of Machine Learning Research*. 2011;12:2825–2830.
54. Feinberg M. *Foundations of chemical reaction network theory*. 2019;.
55. Kidger P. *On Neural Differential Equations*; 2022.
56. Chen HL, Doty D, Reeves W, Soloveichik D. Rate-independent computation in continuous chemical reaction networks. *J ACM*. 2023;70(3):1–61.
57. Zhang DY. Cooperative hybridization of oligonucleotides. *J Am Chem Soc*. 2011;133(4):1077–1086.
58. Song T, Gopalkrishnan N, Eshra A, Garg S, Mokhtar R, Bui H, et al. Improving the performance of DNA strand displacement circuits by shadow cancellation. *ACS Nano*. 2018;12(11):11689–11697.
59. Yurke B, Turberfield AJ, Mills Jr AP, Simmel FC, Neumann JL. A DNA-fuelled molecular machine made of DNA. *Nature*. 2000;406(6796):605–608.
60. Zhang DY, Seelig G. Dynamic DNA nanotechnology using strand-displacement reactions. *Nat Chem*. 2011;3(2):103–113.
61. Baccouche A, Montagne K, Padirac A, Fujii T, Rondelez Y. Dynamic DNA-toolbox reaction circuits: A walkthrough. *Methods*. 2014;67(2):234–249.
62. Shah S, Song T, Song X, Yang M, Reif JH. Implementing arbitrary CRNs using strand displacing polymerase. In: *International Conference on DNA Computing and Molecular Programming*. Springer; 2019. p. 21–36.
63. Rodriguez KR, Sarraf N, Qian L. A Loser-Take-All DNA Circuit. *ACS Synthetic Biology*. 2021;10(11):2878–2885.
64. Lapteva AP, Sarraf N, Qian L. DNA Strand-Displacement Temporal Logic Circuits. *J Am Chem Soc*. 2022;144(27):12443–12449.
65. Zhu S, Zhang Q. *Implementing Feedforward Neural Network Using DNA Strand Displacement Reactions*; 2021.

66. Lv H, Li Q, Shi J, Fan C, Wang F. Biocomputing based on DNA strand displacement reactions. *ChemPhysChem*. 2021;22(12):1151–1166.
67. Milenkovic O, Kashyap N. On the design of codes for DNA computing. In: *International Workshop on Coding and Cryptography*. Springer; 2005. p. 100–119.
68. Reynaldo LP, Vologodskii AV, Neri BP, Lyamichev VI. The kinetics of oligonucleotide replacements. *J Mol Biol*. 2000;297(2):511–520.
69. Wang B, Thachuk C, Ellington AD, Winfree E, Soloveichik D. Effective design principles for leakless strand displacement systems. *Proc Natl Acad Sci*. 2018;115(52):E12182–E12191.
70. Thachuk C, Winfree E, Soloveichik D. *International Workshop on DNA-Based Computers*. Springer; 2015.
71. Zhang M, Yancey C, Zhang C, Wang J, Ma Q, Yang L, et al. A DNA circuit that records molecular events. *Science Advances*. 2024;10(14):eadn3329.
72. Liu X, Zhang X, Yao Y, Shi P, Zeng C, Zhang Q. Construction of DNA-based molecular circuits using normally open and normally closed switches driven by lambda exonuclease. *Nanoscale*. 2023;15(17):7755–7764.
73. Fern J, Scalise D, Cangialosi A, Howie D, Potters L, Schulman R. DNA strand-displacement timer circuits. *ACS synthetic biology*. 2017;6(2):190–193.
74. Cardelli L. Two-domain DNA strand displacement. *Math Struct Comput Sci*. 2013;23(2):247–271.
75. Poole W, Ortiz-Munoz A, Behera A, Jones NS, Ouldrige TE, Winfree E, et al. Chemical boltzmann machines. In: *DNA Computing and Molecular Programming: 23rd International Conference, DNA 23, Austin, TX, USA, September 24–28, 2017, Proceedings 23*. Springer; 2017. p. 210–231.
76. Singh A, Wiuf C, Behera A, Gopalkrishnan M. *DNA Computing and Molecular Programming*. Springer; 2019.
77. Mikolov T, Chen K, Corrado G, Dean J. Efficient Estimation of Word Representations in Vector Space; 2013.
78. Debnath M, Prasad GB, Bisen PS. *Molecular diagnostics: promises and possibilities*. Springer Science & Business Media; 2010.
79. Tjong V, Tang L, Zauscher S, Chilkoti A. “Smart” DNA interfaces. *Chemical Society Reviews*. 2014;43(5):1612–1626.
80. Zhang J, Salaita K. Smart nucleic acids as future therapeutics. *Trends in Biotechnology*. 2021;39(12):1289–1307.
81. Stayton P, El-Sayed M, Murthy N, Bulmus V, Lackey C, Cheung C, et al. ‘Smart’ delivery systems for biomolecular therapeutics. *Orthodontics & craniofacial research*. 2005;8(3):219–225.
82. Yang L, Zhao Y, Xu X, Xu K, Zhang M, Huang K, et al. An intelligent DNA nanorobot for autonomous anticoagulation. *Angewandte Chemie International Edition*. 2020;59(40):17697–17704.
83. Wang Y, Chen-Mayfield TJ, Li Z, Younis MH, Cai W, Hu Q. Harnessing DNA for immunotherapy: Cancer, infectious diseases, and beyond. *Advanced functional materials*. 2022;32(37):2112273.
84. Zhao N, Chen Y, Chen G, Xiao Z. Artificial cells based on DNA nanotechnology. *ACS Applied Bio Materials*. 2020;3(7):3928–3934.
85. Leathers A, Walczak M, Brady RA, Al Samad A, Kotar J, Booth MJ, et al. Reaction–diffusion patterning of DNA-based artificial cells. *Journal of the American Chemical Society*. 2022;144(38):17468–17476.